Electronic Supplementary Material (ESI) for Environmental Science: Nano.

Supplementary Information

Lattice-Strained Nickel Hydroxide Nanosheets for Boosted Diluted CO_2 Photoreduction

Shujie Liang[a†], Bin Han[a†], Xinwen Ou[a], Xucun Ye[a], Weiyi Chen[a], Hong Deng[a,b*],

Chen Tian[a], Zhang Lin[a, c]

[a] School of Environment and Energy, Guangdong Provincial Key Laboratory of Solid Wastes Pollution Control and Recycling, South China University of Technology, Guangzhou, Guangdong 510006, China

[b] Guangdong Engineering and Technology Research Center for Environmental Nanomaterials, South China University of Technology, Guangzhou, Guangdong 510006, China

[c] School of Metallurgy and Environment, Central South University, Changsha 410083, PR China

† These authors contributed equally to this work.

* Correspondence Author: *Prof.* Hong Deng; E-mail: dengh2016@scut.edu.cn

1. Experimental

1.1 Materials

Nickel nitrate hexahydrate ($Ni(NO_3)_2\cdot 6H_2O$), nickel chloride hexahydrate ($NiCl_2\cdot 6H_2O$), ammonia metavanadate (NH_4VO_3), hexamethylenetetramine (HMT, $C_6H_{12}N_4$), sodium dodecyl sulfate (SDS, $C_{12}H_{25}SO_4Na$), sodium orthavanadium (Na_3VO_4), acetonitrile (MeCN), and triethanolamine (TEOA) were bought from Aladdin Chemicals. $[Ru(bpy)_3]Cl_2\cdot 6H_2O$ (abbreviated as Ru, bpy = 2'2'-bipyridine) were purchased from Sinopharm Chemical Reagent Co., Ltd. Deionized water (18 MΩ·cm) was used throughout the experiments.

1.2 Materials synthesis

Synthesis of pristine $Ni(OH)_2$ NS. Pristine $Ni(OH)_2$ NS were synthesized by the reported method with slight modification [1, 2]. Three aqueous solutions, 0.5 M $Ni(NO_3)_2\cdot 6H_2O$, 0.25 M SDS and 1M HMT were firstly prepared separately. Then, Ni^{2+} (2 mL), SDS (20 mL), HMT (6 mL), and 22 mL DI water were mixed. After it was stirred vigorously for 1 h at room temperature, the mixture was sealed in a Teflon-lined stainless-steel autoclave of 100 mL capacity, kept at 120 ^{o}C for 24 h, and then allowed to cool down to room temperature. After the reaction, the precipitates were centrifuged, washed with water several times, and vacuum freeze-drying for 48 h to obtain the $Ni(OH)_2$ NS.

Lattice-strained $Ni(OH)_2$ with various vanadium. The X% V-doped $Ni(OH)_2$ NS were prepared similarly to the process of the $Ni(OH)_2$ NS. Three aqueous solutions, 0.5 M $Ni(NO_3)_2 \cdot 6H_2O$ with a certain amount of NH_4VO_3, 0.25 M SDS, and 1 M HMT were firstly prepared separately. Then, Ni^{2+} (2 mL), SDS (20 mL), HMT (6 mL), and 22 mL DI water were mixed. After it was stirred vigorously for 1 h at room temperature, the mixture was sealed in a Teflon-lined stainless-steel autoclave of 100 mL capacity, kept at 120 ^oC for 24 h, and then allowed to cool down to room temperature. After the reaction, the precipitates were centrifuged, washed with water for several times, and then vacuum freeze-drying for 48 h to obtain the V-doped $Ni(OH)_2$ NS. The doped V atoms in the host $Ni(OH)_2$ was controlled by regulating the molar ratio of V/Ni salts (5:100, 10:100, 15:100, 20:100, and 100:100 named 5%, 10%, 15%, 20% and 100% V-$Ni(OH)_2$ NS, respectively) in the precursor solution.

Synthesis of $Ni_3V_2O_8$. In order to investigate the microstructure of the V-doped $Ni(OH)_2$ NS, $Ni_3V_2O_8$ were prepared as reference materials. 2 mmol $NiCl_2 \cdot 6H_2O$ and 1 mmol Na_3VO_4 were dissolved in 50 mL deionized water. Then 3 mL liquid ammonia was added to the dispersion to form a clear solution. The obtained blue solution was transferred into a Teflon-lined stainless steel autoclave and heated at 180 ^oC for 20 h. After the completion of the reaction, the hydrothermal reactor was cooled down naturally to room temperature. The precipitate was centrifuged and washed several times with water and absolute ethanol and dried at 60 ^oC for 8 h for 24 h to obtain $Ni_3V_2O_8$.

1.3 Material Characterization

The powder X-ray diffraction (XRD) patterns of the samples were collected on a Bruker D8 Advance Powder X-ray diffractometer (40 kV, 40 mA) using Cu Kα radiation in the 2θ ranging from 2 to 70° at a scan rate of 0.02° per second. Field-emission scanning electron microscopy (FE-SEM) was recorded to determine the morphology of the samples on a HITACHI SU8100 instrument equipped with an X-ray energy-dispersive spectrometer (EDS). The transmission electron microscopy (TEM) images and high-resolution transmission electron microscopy (HRTEM) images were obtained using a JEOL model JEM 2010 EX instrument at an acceleration voltage of 200 kV. X-ray photoelectron spectroscopy (XPS) measurements were performed using a Thermo Scientific ESCA Lab250 spectrometer, and all of the binding energies were calibrated by the C 1s peak at 284.6 eV. The Fourier transformed infrared spectroscopy (FTIR) was performed using a Nicolet Nexus 670 FT-IR spectrophotometer at a resolution of 4 cm^{-1} in 400 to 4000 cm^{-1} regions. CO_2 temperature-programmed desorption (TPD) experiments were performed at a Micromeritics AutoChem II 2920 instrument. The Brunauer-Emmett-Teller (BET) surface area and porous structure were analyzed by N_2 adsorption/desorption isotherms method with a Micromeritics ASAP 2020 analyzer. Additionally, the CO_2 adsorption isotherms were also analyzed using a Micromeritics ASAP 2020 analyzer at 298 K. All of the samples were degassed at 433 K for 8 h prior to the sorption measurements. EPR tests were carried out using an ESR spectrometer (JEOL, JES FA300) at 77 K. Photocatalysis tests were put in the PCX50B Discover multi-channel parallel photocatalytic reaction system (Perfect Light Co., Ltd.)

with a 5 W white LED light (400 nm ≤ λ ≤ 800 nm). The $^{13}CO_2$ isotopic experiment was conducted by GC-MS system (Agilent 7890B-5977A). The time-resolved photoluminescence measurements (TRPL) and photoluminescence (PL) were carried out on an Edinburgh FL/FS900 spectrophotometer at room temperature. Electrochemical impedance spectra (EIS), linear-sweep voltammogram (LSV) and Mott−Schottky plots were tested by a CHI 660E electrochemical workstation. In-situ diffuse reflectance infrared Fourier-transform spectroscopy (DRIFTS) test was conducted on a Nicolet iS50 FTIR spectrometer (Thermo Fisher, USA), which equipped with a Praying Mantis diffuse reflectance accessory (Harrick) and a special specimen chamber with two ZnSe windows and one SiO_2 window. The samples were dried in a vacuum oven at 60 ^{o}C overnight. Then degassed catalysts were sealed in the chamber, and purged with Ar to remove the adsorbed air. Lastly, in situ DRIFTS spectra under dark and irradiation taken place in a reaction system in the CO_2/H_2O vapor.

1.4 X-ray absorption spectroscopy (XAS) spectra Collection and Analysis.

Raw XAS data were obtained from the Beijing Synchrotron Radiation Facility at 1W1B. The storage rings energy is 2.5 GeV with current between 160 and 250 mA. Ni K-edge EXAFS was collected by transmission mode with appropriate absorption edge jump in the range from 8137 eV to 9122 eV. V K-edge data were collected in the range from 5269 eV to 6224 eV in fluorescence mode with appropriate absorption edge jump and with a step-size of 0.7 eV at the near edge.

The XAS raw data were processed by standard procedures with the ATHENA and ATHENA program in IFEFFIT software including energy calibration, data alignment, background subtraction, normalization, and Fourier transformation [3]. Edge step normalization for each spectrum was performed by subtracting the pre-edge and post-edge backgrounds. k^3-weighted $\chi(k)$ data in the k-space ranging from 2.0 – 12.0 $Å^{-1}$ for Ni and 2.5 - 11.5 $Å^{-1}$ for V were Fourier transformed to real (R) space using a hanning window (dk = 1.0 $Å^{-1}$) to separate the EXAFS contributions from different coordination shells. Then ARTEMIS with the least-squares curve parameter were fitted to obtain the quantitative structural parameters around Ni and V atoms. Effective scattering amplitudes and phase-shifts for the Ni-O and V-O pairs were calculated with the ab initio code FEFF 8.0. A nonlinear least-squares algorithm was applied for the first-shell curve fitting of EXAFS in R-space between 1.0 and 2.0 Å for the Ni and V K-edge. The amplitude reduction factor, the atomic structure parameters of CN (coordination number), R (Å) (bond distance), Debye-Waller factor (σ^2) and edge-energy shift (ΔE) were estimated by fitting analysis employing the Artemis module implemented in the IFEFFIT package.

1.5 Photocatalytic CO_2 reduction process.

Photocatalytic CO_2 reduction was carried out on the multi-channel parallel photocatalytic reaction system in a liquid-solid reaction system in a 60 mL quartz reactor at ambient temperature under atmospheric pressure. 1.0 mg catalyst, 7.5 mg $[Ru(bpy)_3]Cl_2\cdot 6H_2O$ and 6 mL mixed $MeCN/H_2O/TEOA$ solution (V/V/V: 3/2/1) were added in a gas-closed quartz reactor. Then the reactor was evacuated and purged with a CO_2/Ar mixture with various ratio for several times to remove the dissolved air. After that, the reactor was put in the PCX50B Discover multi-channel parallel photocatalytic reaction system (Perfect Light Co., Ltd.) with a 5 W white LED light (400 nm $\leq \lambda \leq$ 800 nm). During the photocatalytic process, the reaction system was kept with continuous magnetic stirring and constant room temperature by the electronic fans. After a certain photocatalytic reaction time, the product gases were determined and quantified by gas chromatography (GC-7890B, Agilent). When it comes to the recycling tests, the catalyst was recollected by high centrifugation and reacted as the above photocatalytic process.

The selectivity for CO was calculated using the equation below:

$$Selectivity\ of\ CO = \frac{n_{co}}{n_{co} + n_{H_2}} \qquad (1)$$

The apparent quantum efficiency (*A.Q.E.*) was determined under the similar photocatalytic reaction using a monochromatic bandpass filter. The incident light flux was measured by an optical power meter (Ushio spectroradiometer, USR-40), which was determined to be 32.3 mW·cm^{-2}. The illuminated area was estimated to be 3.0 cm^2. So, *A.Q.E.* was calculated by the following equation:

$$A.Q.E.(\%) = \frac{number\ of\ produced\ CO\ molecules \times 2}{number\ of\ incident\ electrons} \times 100\% \qquad (2)$$

The turnover number (TON) was calculated as the moles of product divided by the moles of Ni atoms:

$$TON = \frac{n_{CO}}{n_{Ni}} \qquad (3)$$

The conversion rates of CO_2 were collected by as the moles of CO and the moles of initial CO_2:

$$Conversion\ rates\ of\ CO_2 = \frac{n_{CO}}{n_{CO_2}} \times 100\% \qquad (4)$$

1.6 Electrochemical measurements.

Electrochemical measurements were performed in a gas-tight cell with a three-electrode system at an electrochemical station. The Ag/AgCl electrode and Pt plate serve as reference and counter electrode, respectively. The working electrode was prepared by a typical process. 3 mg as-prepared sample and 60 μL Nafion solution were dispersed in 1 mL water-EtOH (1:1, V: V) by sonicating for 0.5 h to form a homogeneous ink. 100 μL ink was loaded on onto a FTO electrode with 1.0 × 1.0 cm^2. LSV test was performed in CO_2-saturated 0.5 M $KHCO_3$ solution and Ar-saturated 0.5 M $KHCO_3$ solution with a scan rate of 10 mV/s. EIS measurements were tested by A. C. Impedance technique with 5 mV amplitude in a frequency range from 100 KHz to 10 mHz. Mott-Schottky measurements were carried out in 0.2 M Na_2SO_4 aqueous solution at frequencies of 500, 1000, and 1500 Hz, respectively.

2. Supplementary Figures

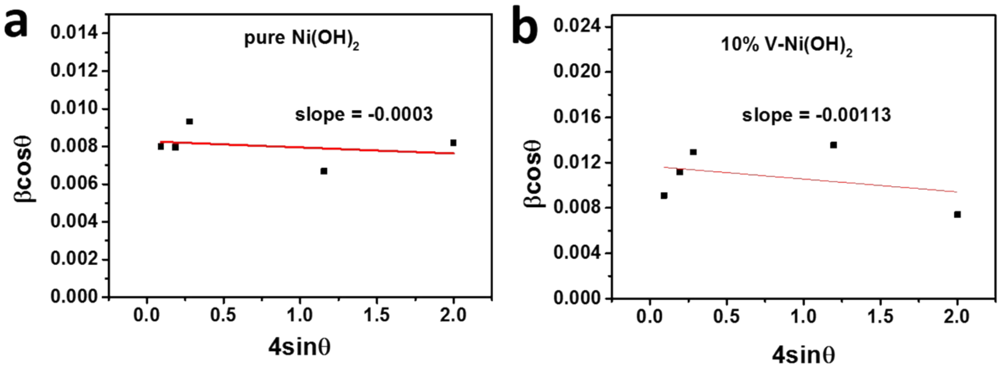

Fig. S1 The W-H analysis of pure Ni(OH)$_2$ NS and 10%-V-Ni(OH)$_2$ NS.

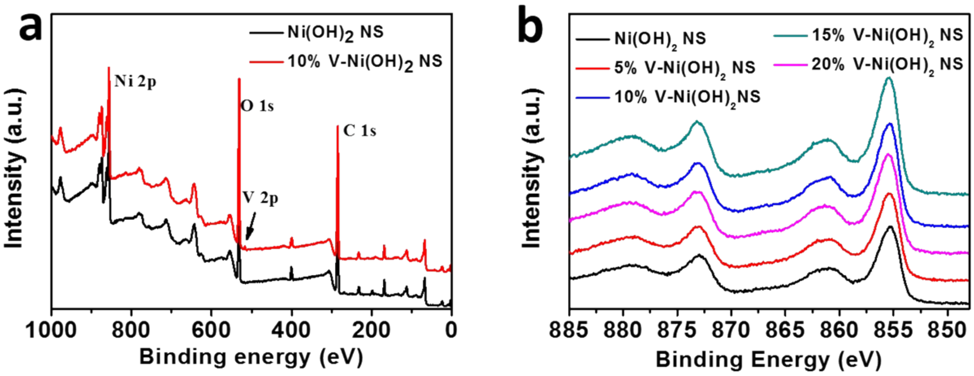

Fig. S2 (a) XPS survey spectrum, and (b) Ni 2p spectra of Ni(OH)$_2$ nanosheets with different V doping amount.

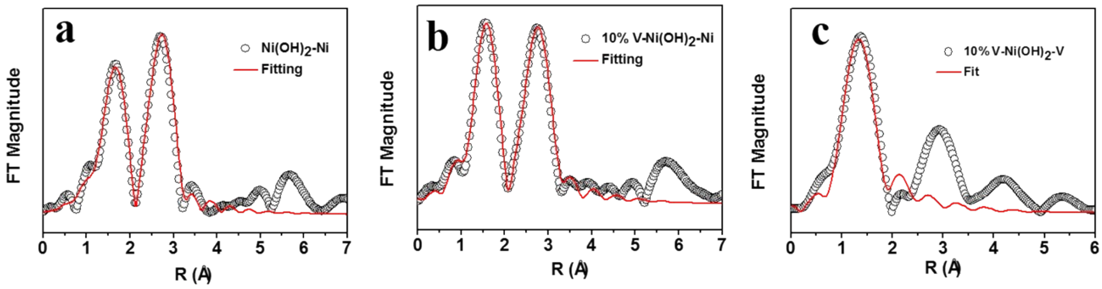

Fig. S3 The fitting results of EXAFS spectra. (a) EXAFS curves-fitting result of the Ni K-edge of $Ni(OH)_2$ nanosheets. (b) EXAFS curves-fitting result of the of Ni K-edge for 10% V-$Ni(OH)_2$ nanosheets. (c) EXAFS curves-fitting result of the of V K-edge for 10% V-$Ni(OH)_2$ nanosheets.

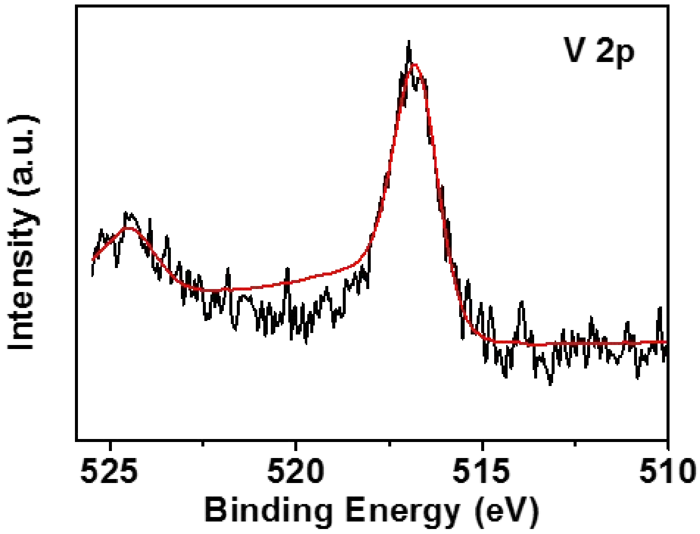

Fig. S4 V 2p of the 10% V-$Ni(OH)_2$ nanosheets.

Note: The V 2p XPS analysis in Fig. S5 in 10% V-$Ni(OH)_2$ NS has binding energies of 517.0 eV and 524.5 eV, corresponding to the V^{5+} phase.[4]

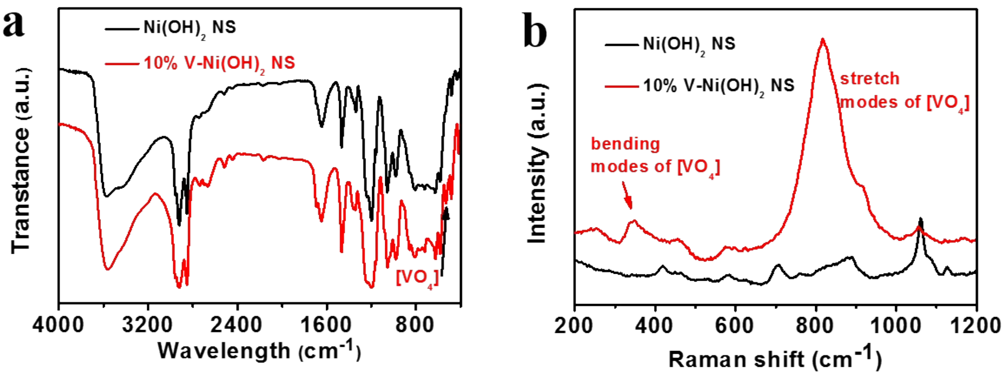

Fig. S5 (a) Fourier transform infrared (FT-IR) spectra, and (b) Raman spectra of the $Ni(OH)_2$ nanosheets and 10% V-$Ni(OH)_2$ nanosheets.

Note: As revealed in Fig. S8, the obvious vibration bands at about 650 cm^{-1} are attributed to tetrahedral $[VO_4]$.[5] In addition, the Raman spectra of 10% V-$Ni(OH)_2$ nanosheets with the distinct peaks at about 800 cm^{-1} and 350 cm^{-1}, which could be attributed to the stretch modes and bending modes of $[VO_4]$.[6] All data support the existence of $[VO_4]$.

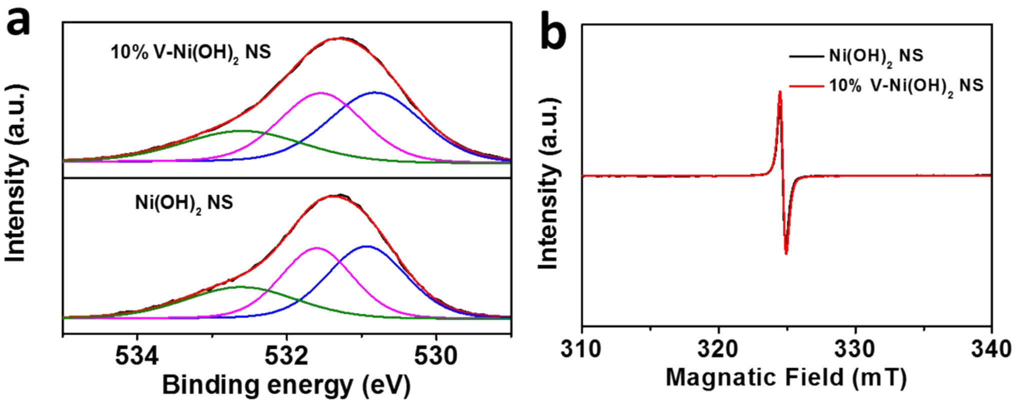

Fig. S6 (a) O 1s, and (b) EPR spectra of $Ni(OH)_2$ nanosheets with different V doping amount.

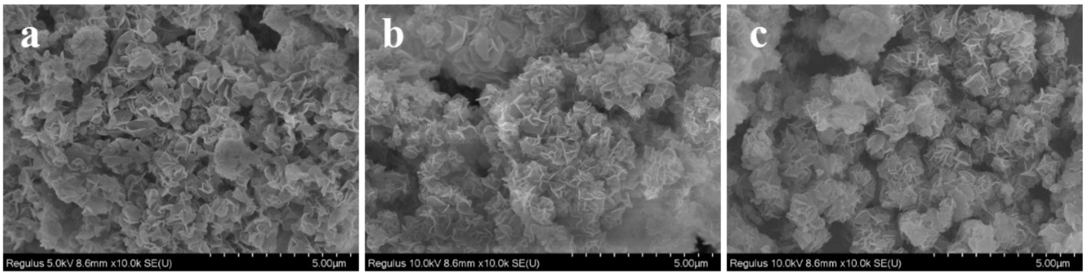

$Ni(OH)_2$ NS **5% V-$Ni(OH)_2$ NS** **10% V-$Ni(OH)_2$ NS**

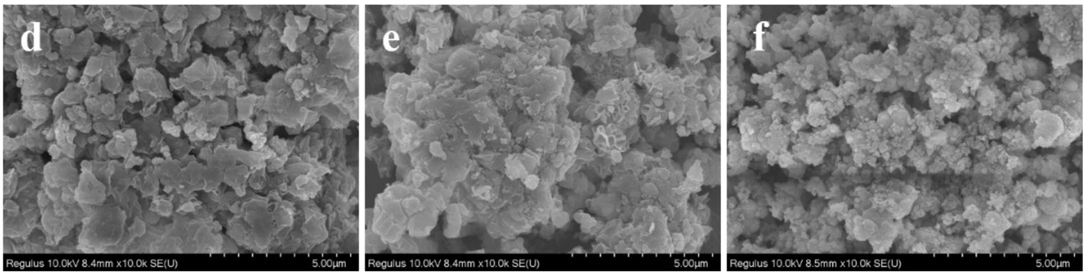

15% V-$Ni(OH)_2$ NS **20% V-$Ni(OH)_2$ NS** **100% V-$Ni(OH)_2$ NS**

Fig. S7 Morphology evolution of $Ni(OH)_2$ with different V-doping.

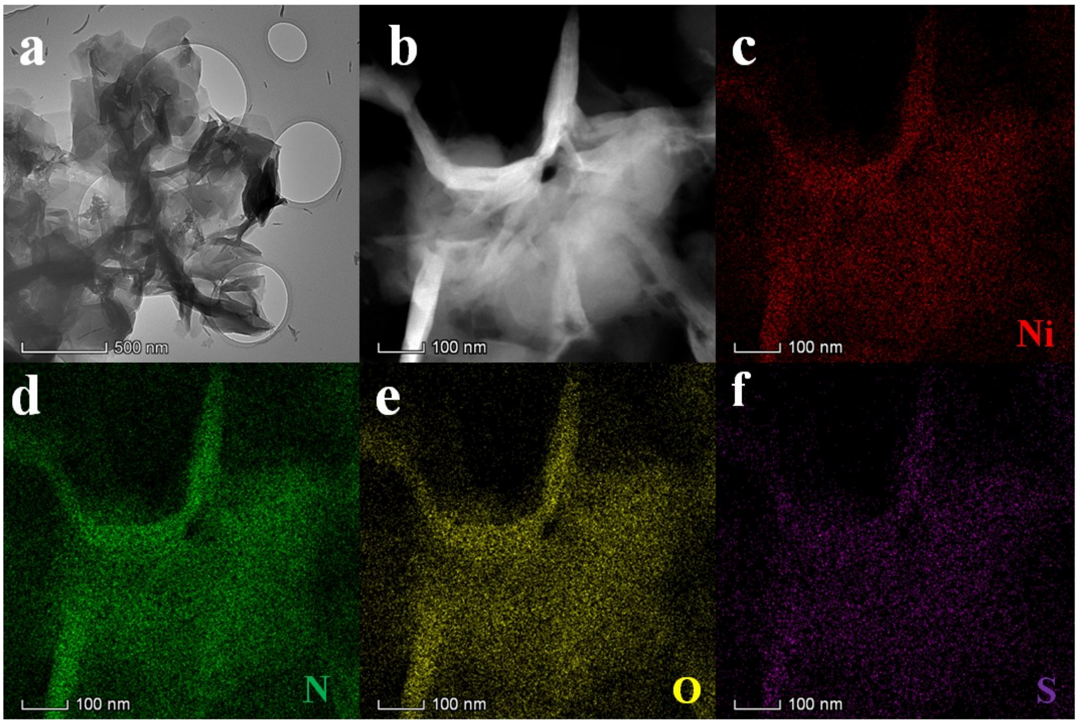

Fig. S8 (a) TEM image, (b) HAADF-STEM image and (c-f) related EDX elemental mappings of Ni, N, O, and S of $Ni(OH)_2$ NS.

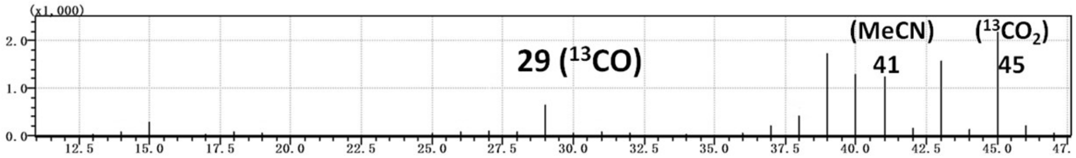

Fig. S9 GC-Mass spectra of photogenerated ^{13}CO (m/z) produced over 10% V-Ni(OH)$_2$ NS.

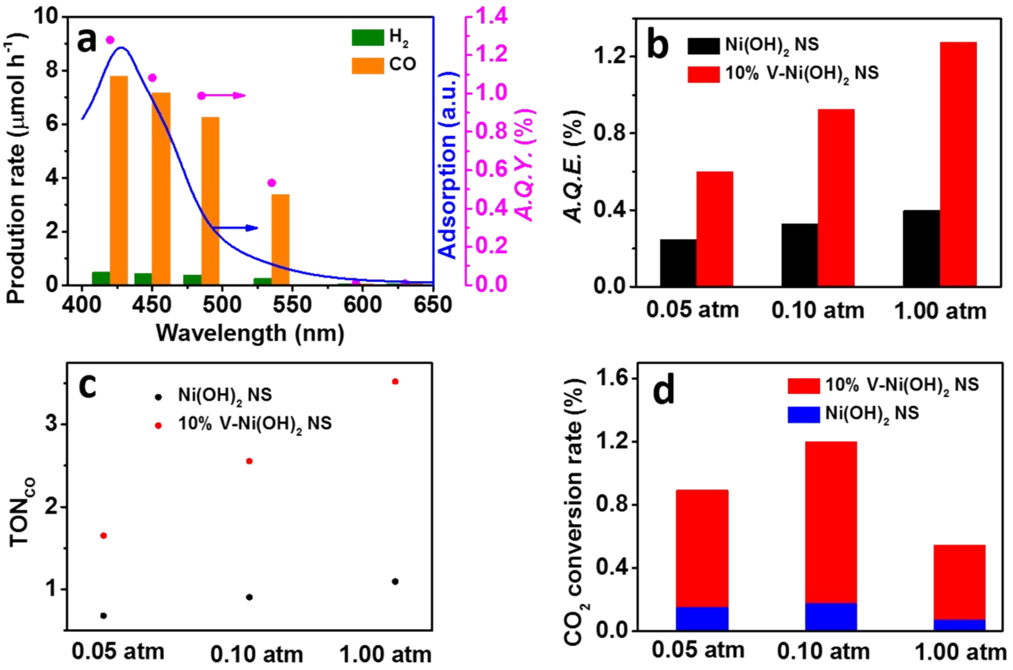

Fig. S10 (a) Relationship between CO_2 photoreduction performance and wavelength during the first hour. (b) *A.Q.E.*, (c) TON, and (d) CO_2 conversion rate of CO over 10% V-Ni(OH)$_2$ NS and Ni(OH)$_2$ NS at 420 nm in different CO_2 concentration within 2 h.

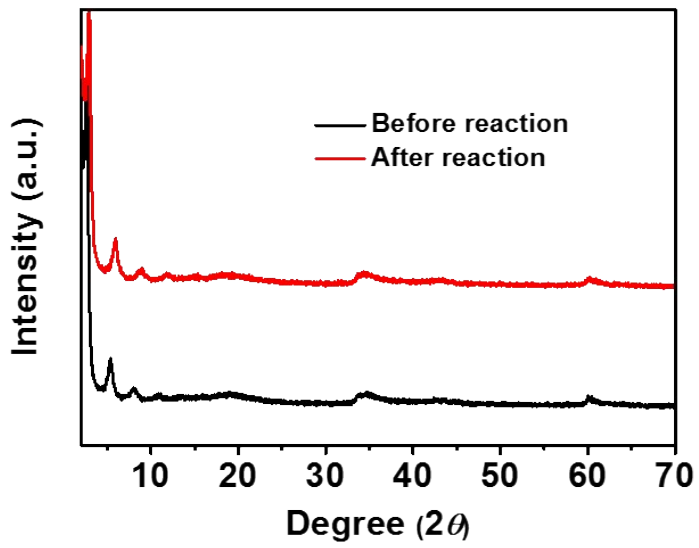

Fig. S11 XRD spectra patterns of the 10% V-Ni(OH)$_2$ NS and Ni(OH)$_2$ NS before and after CO$_2$ photoreduction reaction.

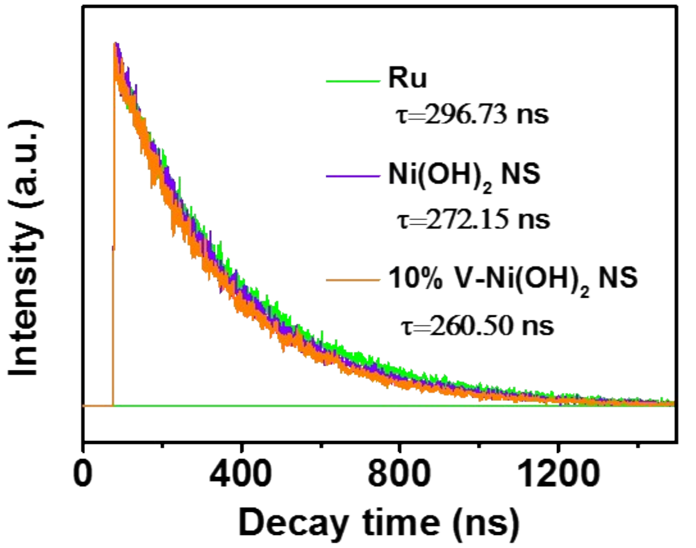

Fig. S12 Time-resolved transient PL decay spectra of the CO$_2$ photoreduction systems.

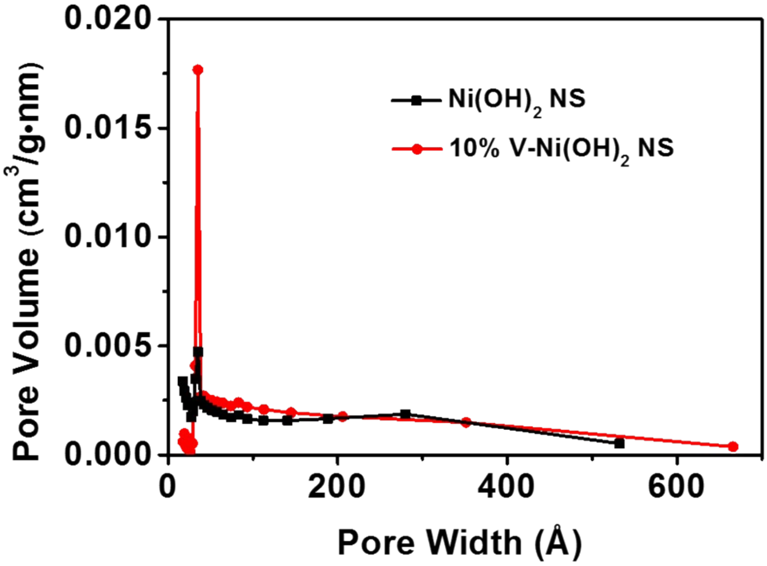

Fig. S13 Pore size distribution of the 10% V-Ni(OH)$_2$ NS and Ni(OH)$_2$ NS.

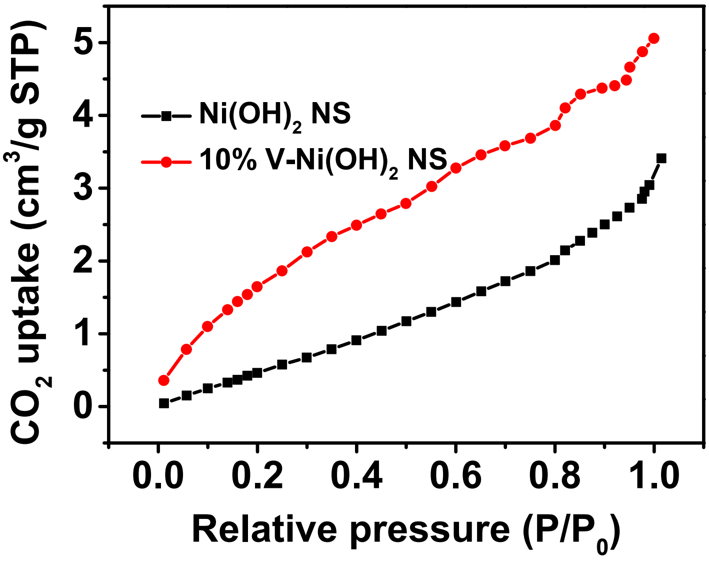

Fig. S14 CO_2 adsorption plots of the 10% V-Ni(OH)$_2$ NS and Ni(OH)$_2$ NS.

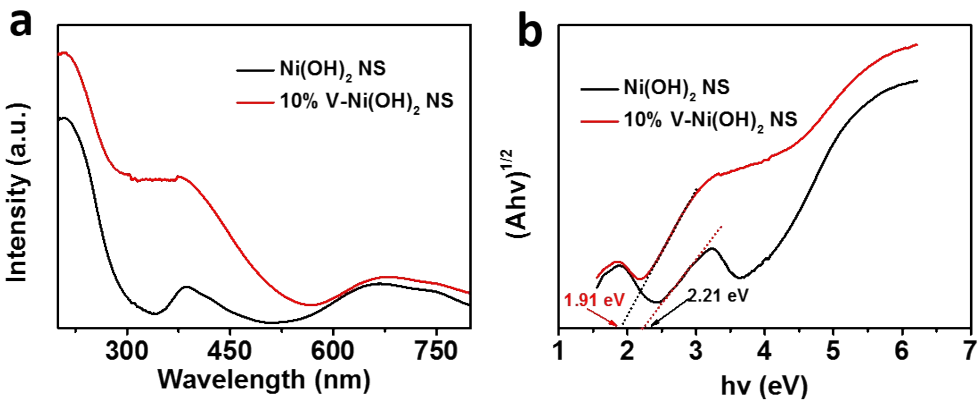

Fig. S15 (a) DRS and (b) their Tauc plots of $Ni(OH)_2$ NS and 10% V-$Ni(OH)_2$ NS.

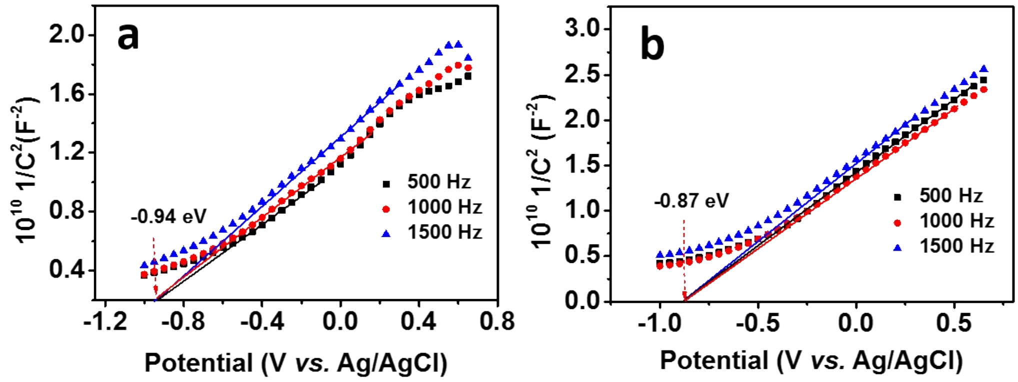

Fig. S16 Mott–Schottky plots of (a) 10% V-$Ni(OH)_2$ NS, and (b)$Ni(OH)_2$ NS measured at frequency of 500 Hz, 1000 HZ and 1500 Hz, respectively.

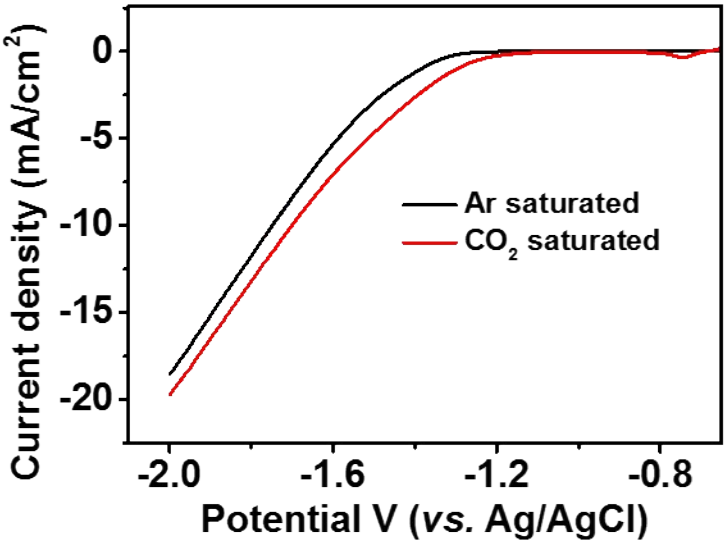

Fig. S17 LSV plots of Ni(OH)$_2$ NS in Ar or CO$_2$-saturated KHCO$_3$ solution.

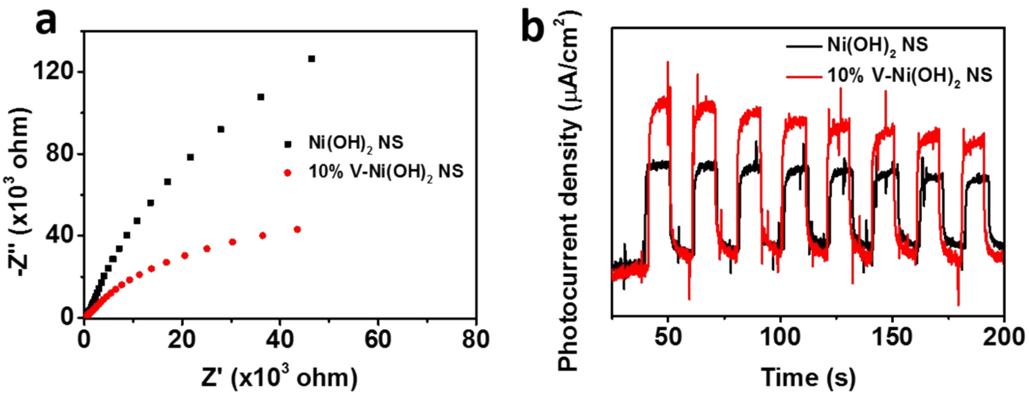

Fig. S18 (a) Nyquist plots and (b) I–t curves of Ni(OH)$_2$ NS and 10% V-Ni(OH)$_2$ NS.

Supplementary Tables

Supplementary Table 1. ICP-OES analysis data for the vanadium and Nickel atomic ratios of metals of the as-prepared catalyst.

Catalyst	**Feedstock** **(V: Ni in molar)**	**ICP-OES** **(V: Ni in molar)**
$Ni(OH)_2$	0:100	0.1:100
5% V- $Ni(OH)_2$	5:100	4.6:100
10% V- $Ni(OH)_2$	10:100	9.8:100
15% V- $Ni(OH)_2$	15:100	16.9:100
20% V- $Ni(OH)_2$	20:100	21.6:100
50% V- $Ni(OH)_2$	50:100	44.2:100

Supplementary Table 2. EXAFS fitting results for the structural parameters around Ni for the 10% V-Ni(OH)$_2$ nanosheets and Ni(OH)$_2$ nanosheets (R: range from 1.0 to 3.0 Å). The first shell of Ni(OH)$_2$ NS represent the nearest-neighbour Ni-O coordination sphere with an average distance of 2.04 **Å**, and coordination number of 5.40. However, distinct variations were observed after intruducing Vanadium into Ni(OH)$_2$ NS. The first shell in the Ni K-edge EXAFS spectrum of 10% V-Ni(OH)$_2$ NS is at a distance of 2.03 **Å**, with a coordination number of 5.24, which indicates lattice distortion and shrinkage of the lattice occur in the 10% V-Ni(OH)$_2$ nanosheets.

Sample	**Scattering pair**	**CN**	**R(Å)**	**σ^2 (Å^{-2})**	**ΔE**	**R-factor**
10% V-Ni(OH)$_2$	Ni-O	5.24	2.03	0.00693	-6.709	0.0056
Ni(OH)$_2$	Ni-O	5.57	2.04	0.00613	-4.921	0.0002
10% V-Ni(OH)$_2$	V-O	3.7	1.73	0.00706	10.4	0.0187

CN stands for coordination number; R stands for bonding distance; σ^2 stands for Debye-Waller factor; △E stands for the edge-energy shift.

Supplementary Table 3. Comparison of CO_2 photoreduction activity with other similar photoreduction systems under pure or diluted CO_2 atmosphere.

Catalyst	CO_2 atmosphere	Reaction condition	Photosen-sitizer	Main products (μmol h^{-1})	CO selectivity (%)	*Ref.*
Co_3O_4	1.00 atm	MeCN TEOA	$Ru(bpy)_3^{2+}$	CO: 2.003 H_2:0.595	77.1	7
$MnCo_2O_4$	1.00 atm	MeCN TEOA	$Ru(bpy)_3^{2+}$	CO: 27 H_2:8	77.1	8
$ZnCo_2O_4$	1.00 atm	MeCN TEOA	$Ru(bpy)_3^{2+}$	CO: 25.1 H_2:8.7	74.3	9
NC@$NiCo_2O_4$	1.00 atm	MeCN TEOA	$Ru(bpy)_3^{2+}$	CO: 26.2 H_2:3.4	88.5	10
Co-C composites	1.00 atm	MeCN TEOA	$Ru(bpy)_3^{2+}$	CO: 9.4 H_2:5.2	64.2	11
$CuCo_2O_4$	1.00 atm	MeCN TEOA	$Ru(bpy)_3^{2+}$	CO: 23 H_2:4.9	82.4	12
$CoSn(OH)_6$	1.00 atm	MeCN TEOA	$Ru(bpy)_3^{2+}$	CO: 18.7 H_2:3.0	86.2	13
$NiCo_2O_4$	1.00 atm	MeCN TEOA	$Ru(bpy)_3^{2+}$	CO: 21 H_2:4	84	14
In_2S_3–$CuInS_2$	1.00 atm	MeCN	$Ru(bpy)_3^{2+}$	CO: 19	---	15

		TEOA		H_2: ---		
Co-Co LDHs	1.00 atm	MeCN TEOA	$Ru(bpy)_3^{2+}$	CO: 6.248 H_2:3.53	63.9	16
Co_3O_4NS	1.00 atm	MeCN TEOA	$Ru(bpy)_3^{2+}$	CO: 4.52 H_2:1.53	74.7	17
$NiCo_2O_4$ HCs	1.00 atm	MeCN TEOA	$Ru(bpy)_3^{2+}$	CO: 10.5 H_2:0.74	93.4	18
10% V-$Ni(OH)_2$ NS	**1.00 atm**	**MeCN TEOA**	**$Ru(bpy)_3^{2+}$**	**CO: 6.1 H_2:0.173**	**97.2**	**This work**
10% V-$Ni(OH)_2$ NS	**0.1 atm**	**H_2O/MeCN /TEOA**	**$Ru(bpy)_3^{2+}$**	**CO: 5.9 H_2:0.553**	**91.4**	**This work**
10% V-$Ni(OH)_2$ NS	**0.05 atm**	**H_2O/MeCN /TEOA**	**$Ru(bpy)_3^{2+}$**	**CO: 3.8 H_2:0.546**	**87.4**	**This work**

3. Supplementary References

1. H. Yin, S. Zhao, K. Zhao, A. Muqsit, H. Tang, L. Chang, H. Zhao, Y. Gao and Z. Tang, Ultrathin platinum nanowires grown on single-layered nickel hydroxide with high hydrogen evolution activity, *Nat. Commun.*, 2015, **6**, 6430.
2. S. Ida, D. Shiga, M. Koinuma and Y. Matsumoto, Synthesis of hexagonal nickel hydroxide nanosheets by exfoliation of layered nickel hydroxide intercalated with dodecyl sulfate ions, *J. Am. Chem. Soc.*, 2008, **130**, 14038-14039.
3. B. Ravel and M. Newville, ATHENA, ARTEMIS, HEPHAESTUS: data analysis for X-ray absorption spectroscopy using IFEFFIT, *Journal of Synchrotron Radiation*, 2005, **12**, 537-541.
4. R. Jaiswal, N. Patel, D. C. Kothari and A. Miotello, Improved visible light photocatalytic activity of TiO_2 co-doped with Vanadium and Nitrogen, *Appl. Catal. B*, 2012, **126**, 47-54.
5. J. Liu, Y. Ji, J. Nai, X. Niu, Y. Luo, L. Guo and S. Yang, Ultrathin amorphous cobalt–vanadium hydr(oxy)oxide catalysts for the oxygen evolution reaction, *Energy Environ. Sci.*, 2018, **11**, 1736-1741.
6. S. Gao, B. Gu, X. Jiao, Y. Sun, X. Zu, F. Yang, W. Zhu, C. Wang, Z. Feng, B. Ye and Y. Xie, Highly

efficient and exceptionally durable CO_2 photoreduction to methanol over freestanding defective single-unit-cell bismuth vanadate layers, *J. Am. Chem. Soc.*, 2017, **139**, 3438-3445.

7. C. Gao, Q. Meng, K. Zhao, H. Yin, D. Wang, J. Guo, S. Zhao, L. Chang, M. He, Q. Li, H. Zhao, X. Huang, Y. Gao and Z. Tang, Co_3O_4 hexagonal platelets with controllable facets enabling highly efficient visible-light photocatalytic reduction of CO_2, *Adv. Mater.*, 2016, **28**, 6485-6490.
8. S. Wang, Y. Hou and X. Wang, Development of a stable $MnCo_2O_4$ cocatalyst for photocatalytic CO_2 reduction with visible light, *ACS Appl. Mater. Interfaces*, 2015, **7**, 4327-4335.
9. S. Wang, Z. Ding and X. Wang, A stable $ZnCo_2O_4$ cocatalyst for photocatalytic CO_2 reduction, *Chem. Commun.*, 2015, **51**, 1517-1519.
10. S. Wang, B. Y. Guan and X. W. Lou, Rationally designed hierarchical N-doped carbon@$NiCo_2O_4$ double-shelled nanoboxes for enhanced visible light CO_2 reduction, *Energy Environ. Sci.*, 2018, **11**, 306-310.
11. K. Zhao, S. Zhao, C. Gao, J. Qi, H. Yin, D. Wei, M. F. Mideksa, X. Wang, Y. Gao, Z. Tang and R. Yu, Metallic cobalt–carbon composite as recyclable and robust magnetic photocatalyst for efficient CO_2 reduction, *Small*, 2018, **14**, 1800762.
12. M. Jiang, Y. Gao, Z. Wang and Z. Ding, Photocatalytic CO_2 reduction promoted by a $CuCo_2O_4$ cocatalyst with homogeneous and heterogeneous light harvesters, *Appl. Catal. B*, 2016, **198**, 180-188.
13. X. Lin, Y. Gao, M. Jiang, Y. Zhang, Y. Hou, W. Dai, S. Wang and Z. Ding, Photocatalytic CO_2 reduction promoted by uniform perovskite hydroxide $CoSn(OH)_6$ nanocubes, *Appl. Catal. B*, 2018, **224**, 1009-1016.
14. Z. Wang, M. Jiang, J. Qin, H. Zhou and Z. Ding, Reinforced photocatalytic reduction of CO_2 to CO by a ternary metal oxide $NiCo_2O_4$, *Phys. Chem. Chem. Phys.*, 2015, **17**, 16040-16046.
15. J. Yang, X. Zhu, Z. Mo, J. Yi, J. Yan, J. Deng, Y. Xu, Y. She, J. Qian, H. Xu and H. Li, A multidimensional In_2S_3–$CuInS_2$ heterostructure for photocatalytic carbon dioxide reduction, *Inorg. Chem. Front.*, 2018, **5**, 3163-3169.
16. W. Chen, B. Han, Y. Xie, S. Liang, H. Deng and Z. Lin, Ultrathin Co-Co LDHs nanosheets assembled vertically on MXene: 3D nanoarrays for boosted visible-light-driven CO_2 reduction, *Chem. Eng. J.*, 2014, **25**, 1419-1422.
17. W. Chen, B. Han, C. Tian, X. Liu, S. Liang, H. Deng and Z. Lin, MOFs-derived ultrathin holey Co_3O_4 nanosheets for enhanced visible light CO_2 reduction, *Appl. Catal. B*, 2019, **244**, 996-1003.
18. B. Han, J. Song, S. Liang, W. Chen, H. Deng, X. Ou, Y.-J. Xu and Z. Lin, Hierarchical $NiCo_2O_4$ hollow nanocages for photoreduction of diluted CO_2: adsorption and active sites engineering, *Appl. Catal. B*, 2020, **260**, 118208.